

**Manuscript version: Published Version**

The version presented in WRAP is the published version (Version of Record).

**Persistent WRAP URL:**

<http://wrap.warwick.ac.uk/128986>

**How to cite:**

The repository item page linked to above, will contain details on accessing citation guidance from the publisher.

**Copyright and reuse:**

The Warwick Research Archive Portal (WRAP) makes this work by researchers of the University of Warwick available open access under the following conditions.

Copyright © and all moral rights to the version of the paper presented here belong to the individual author(s) and/or other copyright owners. To the extent reasonable and practicable the material made available in WRAP has been checked for eligibility before being made available.

Copies of full items can be used for personal research or study, educational, or not-for-profit purposes without prior permission or charge. Provided that the authors, title and full bibliographic details are credited, a hyperlink and/or URL is given for the original metadata page and the content is not changed in any way.

**Publisher's statement:**



Please refer to the repository item page, publisher's statement section, for further information.

For more information, please contact the WRAP Team at: [wrap@warwick.ac.uk](mailto:wrap@warwick.ac.uk)

# Modeling and control methodology for an XYZ micro manipulator

Cite as: Rev. Sci. Instrum. **90**, 105007 (2019); <https://doi.org/10.1063/1.5116094>

Submitted: 21 June 2019 . Accepted: 09 October 2019 . Published Online: 23 October 2019

Yanling Tian, Yue Ma, KangKang Lu, Mingxuan Yang, Xiaolu Zhao, Fujun Wang , and Dawei Zhang 



View Online



Export Citation



CrossMark

## ARTICLES YOU MAY BE INTERESTED IN

[A low-noise resonant input transimpedance amplified photodetector](#)

Review of Scientific Instruments **90**, 106106 (2019); <https://doi.org/10.1063/1.5114896>

[Design of a flexure-based mechanism possessing low stiffness and constant force](#)

Review of Scientific Instruments **90**, 105005 (2019); <https://doi.org/10.1063/1.5119276>

[Extending the pulse length of the ISIS H<sup>-</sup> Penning ion source](#)

Review of Scientific Instruments **90**, 103311 (2019); <https://doi.org/10.1063/1.5126729>



Lock-in Amplifiers

Zurich Instruments

Watch the Video

# Modeling and control methodology for an XYZ micro manipulator

Cite as: Rev. Sci. Instrum. 90, 105007 (2019); doi: 10.1063/1.5116094

Submitted: 21 June 2019 • Accepted: 9 October 2019 •

Published Online: 23 October 2019



Yanling Tian,<sup>1,2,a)</sup> Yue Ma,<sup>1</sup> KangKang Lu,<sup>1</sup> Mingxuan Yang,<sup>1</sup> Xiaolu Zhao,<sup>1</sup> Fujun Wang,<sup>1</sup>  and Dawei Zhang<sup>1</sup> 

## AFFILIATIONS

<sup>1</sup>Key Laboratory of Mechanism Theory and Equipment Design of Ministry of Education, School of Mechanical Engineering, Tianjin University, Tianjin 300054, China

<sup>2</sup>School of Engineering, University of Warwick, Coventry CV4 7AL, United Kingdom

<sup>a)</sup>Author to whom correspondence should be addressed: [meytian@tju.edu.cn](mailto:meytian@tju.edu.cn)

## ABSTRACT

This paper presents the modeling and control methodology for a piezoactuated compliant XYZ manipulator toward precision positioning. The manipulator was fabricated using a wire electrical discharge machining technique, and the system identification was conducted to obtain the dynamic model based on the frequency response. To reduce the effects of hysteresis, creep, and external disturbances, a feedforward/feedback hybrid controller is proposed, which contains a dynamic dependent Prandtl-Ishlinskii (DDPI) hysteresis model and a novel sliding mode controller. The DDPI hysteresis model has excellent modeling accuracy at high operating frequencies with consideration of the dynamic characteristics of the micromanipulator. The novel sliding mode controller integrated with uncertainty and disturbance estimation (SMCUE) technique is developed, which has the advantages of fast response, strong robustness, and resistance to chattering. The performance of the DDPI hysteresis model and the novel sliding mode controller is validated and compared using experimental tests. The experimental results indicate that the DDPI model provides better positioning accuracy than the traditional Prandtl-Ishlinskii (P-I) model and the rate-dependent P-I model, and furthermore, the SMCUE controller can improve the response speed without loss of stability, which demonstrates that precision positioning operations can be implemented by the developed manipulator using the proposed control strategy.

Published under license by AIP Publishing. <https://doi.org/10.1063/1.5116094>

## I. INTRODUCTION

With the rapid development of micro/nanotechnology, micro/nanomanipulators capable of precision positioning have played an increasingly important role in micro/nanomanufacturing and packaging, micro/nanomeasurement and manipulation.<sup>1–5</sup> In recent years, micromanipulators actuated by piezoelectric actuators (PEAs) attract considerable attention in various precision engineering applications since PEA provides a number of merits including fast response, high resolution, and large bandwidth.<sup>6</sup> However, inherent hysteresis and creep nonlinearity of the PEAs limit the accuracy of piezoactuated micromanipulators.<sup>7</sup> In addition, external disturbances should also be considered and strictly controlled in micro/nanopositioning applications.<sup>8</sup> Therefore, the modeling and control methodology for micromanipulators is one of the important issues for improving the static and dynamic performance, and thus, it has received extensive attention both in academic and industrial sectors.

Recent efforts have been directed toward the control methodologies including feedforward, feedback, and feedforward/feedback controls for micromanipulators. Based on the inverse hysteresis model of the micromanipulators, the feedforward control provides a simple and effective way to reduce system hysteresis errors, and thus, the accuracy of the system can be improved to some extent. However, the shortcoming of feedforward control is that it usually lacks robustness to environmental changes and external uncertainties.<sup>9</sup> Feedback control is another effective control method for piezoactuated manipulators. Both hysteresis and external disturbance can be reduced/eliminated through closed-loop feedback control. However, the tracking performance of feedback control for piezoactuated micromanipulators will degrade at high frequency-domain due to the drawback of the low gain margin vibration dynamics.<sup>10</sup> Combining the merits of feedforward and feedback controls, the hybrid feedforward/feedback control provides an excellent way for the precision control of micromanipulators.

For feedforward/feedback control, two issues should be considered: feedforward controller design and feedback controller design. As for the feedforward control, a variety of hysteresis models have been proposed to provide a precision output motion for micromanipulators, and these include the Preisach model, the Bouc-Wen model, and the Prandtl-Ishlinskii (P-I) model.<sup>11–13</sup> Among these hysteresis models, the P-I model has been widely utilized due to the simple structure, easy modeling identification, and analytical inverse.<sup>14</sup> Ang *et al.* observed that the hysteresis slope of the PEA was affected linearly by the actuation rate, and they accordingly designed a rate-dependent P-I (RDPI) hysteresis slope model.<sup>15</sup> Qin *et al.* established a novel direct inverse modeling approach to directly obtain the inverse P-I model based on experimental data.<sup>16</sup> For hysteresis modeling, the system dynamic error will seriously deteriorate the performance of the feedforward control, so recent research studies focus on the hysteresis modeling considering the system dynamic performance.<sup>17</sup> Referring to the feedback control, proportional-integral-derivative (PID) controllers have been widely employed in industrial applications.<sup>18</sup> Compared with PID control, advanced control schemes with excellent control precision were proposed, such as adaptive control, robust control, and neural networks control.<sup>19–21</sup> However, computationally expensive calculations limit their applications in high speed and precise positioning.<sup>22</sup> Sliding mode control (SMC), a nonlinear approach, is popularly applied in precision positioning systems due to fast response and strong robustness for the disturbances.<sup>23</sup> However, the chattering phenomenon is still one of the unsolved issues in the SMC system. Many control strategies have been introduced to suppress the chattering phenomenon, such as high-order sliding mode strategy,<sup>24</sup> digital sliding mode scheme,<sup>25</sup> boundary layer method,<sup>26</sup> and uncertainty and disturbance estimation (UDE) technique.<sup>27</sup> Among these proposed techniques, UDE is a simple and effective way to reduce chattering without complex control model, and thus, it is increasingly utilized in SMC implementation.

This paper is motivated to implement the high speed and precision positioning of an XYZ micromanipulator, which is limited by the hysteresis, creep, and external disturbances of the piezoactuated system. In order to overcome the above problems, a hybrid feedforward/feedback controller is designed, which incorporates a dynamic-dependent P-I (DDPI) hysteresis model and a novel sliding mode controller with uncertainty and disturbance estimation (SMCUDE) technique. The DDPI hysteresis model combines a rate-dependent P-I model and a system dynamic model, and it is not only related to the operating frequency but also to the dynamic performance of the system. The developed SMCUDE controller integrates the uncertainty and disturbance estimation technique to achieve excellent dynamic performance. Compared with the traditional SMC, the SMCUDE controller reduces the chattering phenomenon and improves system robustness with fast response capability. The remainder of this paper is organized as follows: the mechanism of the XYZ micro/nanomanipulator is introduced in Sec. II. Section III presents the prototype development and system identification. The design and parameter identification of the DDPI model is described in Sec. IV. The SMCUDE controller is proposed in Sec. V. Experimental tests are implemented in Sec. VI, and the conclusions are drawn in Sec. VII.

## II. MECHANISM OF THE MICROMANIPULATOR

The overall mechanism of the piezoelectric actuated manipulator is shown in Fig. 1. For the sake of high stiffness and compact structure, the Z platform is embedded in the moving platform of the parallel XY positioning stage. The XY stage is composed of four symmetric arms, and each two adjacent arms are orthogonal to reduce parasitic motion and obtain motion decoupling in the X and Y directions. Moreover, the influences of thermal deformation and external vibration can be reduced by utilizing symmetric configuration. To enlarge the motion range of the moving platform, a hybrid amplification mechanism is introduced, which consists of a

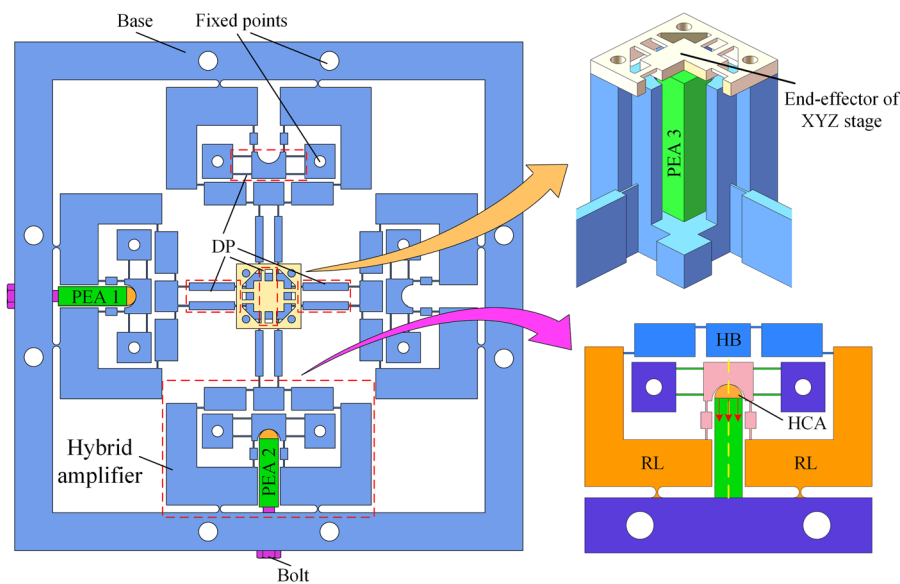


FIG. 1. Mechanism of the XYZ micromanipulator.

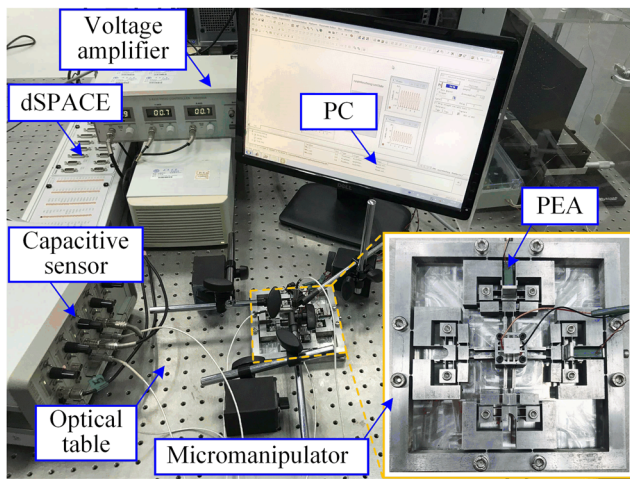


FIG. 2. Experimental setup.

pair of rotational levers (RLs) and a half-bridge (HB) mechanism. The rotational lever mechanism is utilized to obtain displacement amplification and change the motion direction. A pair of rotational levers is symmetrically utilized to counteract lateral parasitic motion, which is connected with a half-bridge mechanism in series to further improve the displacement amplification ratio. To enhance lateral stiffness, the leaf-type double parallelogram (DP) mechanism is incorporated into the input end of the hybrid amplifier. The hybrid

amplification mechanism has a compact structure and a large lateral rigidity with considerable amplification ratio. To protect the PEA from bending and torsional moments, a hemisphere ceramic adapter (HCA) is applied to transform the concentrated force into distributed force on the top surface of PEA. Besides, the input end of the mechanism is designed as a concave surface cooperated with the hemisphere surface to provide excellent automatic centering and locating functions. The hybrid amplification mechanism and the Z stage are connected by double parallelogram mechanisms, which have a large lateral stiffness to act as a guiding mechanism suppressing lateral motion error. Meanwhile, the mechanism has a low axial stiffness to isolate the interaction of drivers in different directions and reduce the input coupling error.

### III. PROTOTYPE FABRICATION AND SYSTEM IDENTIFICATION

#### A. Prototype fabrication

The prototype of the XYZ micromanipulator system is illustrated in Fig. 2. The manipulator was fabricated of aluminum alloy T7075 by a wire electrical discharge machining (WEDM) technique. The overall dimension of the manipulator is  $134 \times 134 \times 27 \text{ mm}^3$ . The manipulator is driven by three PEAs (PSt150/5  $\times$  5  $\times$  20 L from COREMORROW, Inc.) to achieve high precision input displacement. A dSPACE DS1103 R&D control board is utilized to implement control signals. The analog voltages were amplified by a THORLABS voltage amplifier by 10 times to drive PEAs. The displacements of the manipulator are measured by three capacitive

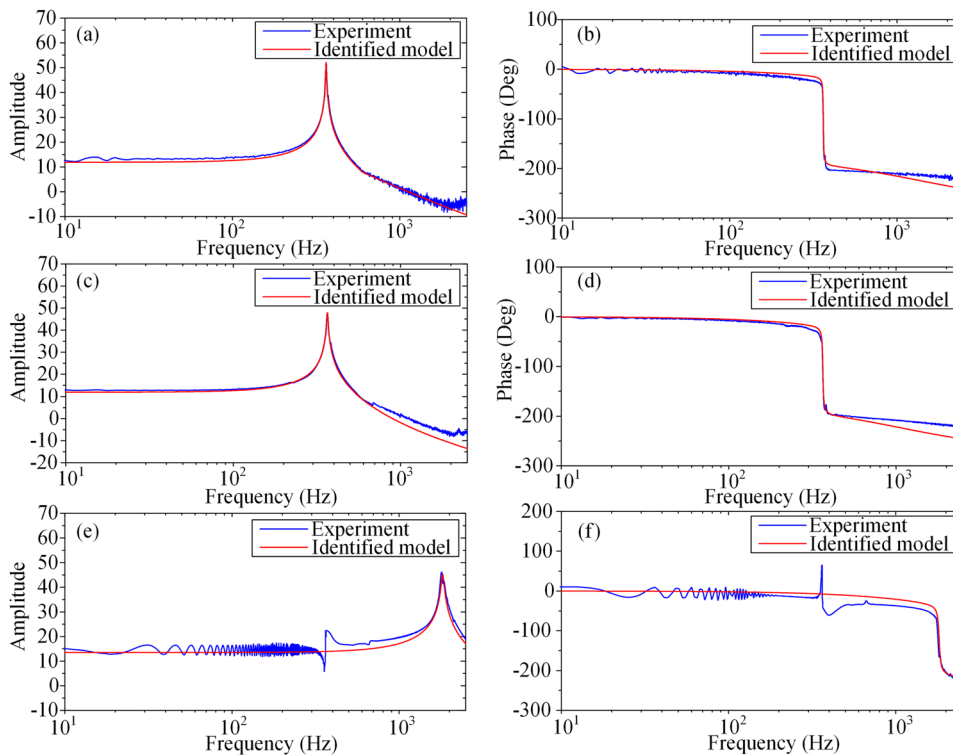


FIG. 3. System identification results of the manipulator. [(a) and (b)] X-axis. [(c) and (d)] Y-axis. [(e) and (f)] Z-axis.



sensors (C8-2.0 Lion, Inc.), whose output signals are collected in real time by a computer through the dSPACE controller. In order to reduce external disturbance, the entire experiments were conducted on a vibration isolation Newport RS-4000 optical table.

## B. System parameter identification

In order to design the manipulator controller, the frequency response based on the system parameter identification technique was conducted to obtain the dynamic model of the micromanipulator. The PEA was actuated by the dSPACE controller using a sinusoidal wave sweep with the amplitude of 0.1 V and the frequency varying from 0.1 Hz to 2500 Hz. The resonance amplitude was measured by capacitive sensors at a sampling rate of 10 kHz. Then, the collected data were processed using a Matlab System Identification Toolbox, and the results are shown in Fig. 3. It can be observed that the natural frequencies of the manipulator along the X, Y, and Z directions are 362.8 Hz, 365.9 Hz, and 1861.4 Hz, respectively, and the identification results are in good agreement with the experimental results. According to the identification results, the transfer functions of the micromanipulator can also be obtained from the input-output relationship and given as follows:

$$\begin{aligned} G_x(s) &= \frac{-2.068 \times 10^7}{s^2 + 22.94s + 5.178 \times 10^6}, \\ G_y(s) &= \frac{-2.101 \times 10^7}{s^2 + 37.62s + 5.237 \times 10^6}, \\ G_z(s) &= \frac{-5.505 \times 10^8}{s^2 + 113.7s + 1.3 \times 10^8}, \end{aligned} \quad (1)$$

where  $G_x(s)$ ,  $G_y(s)$ , and  $G_z(s)$  represent the transfer functions of the system along the X, Y, and Z directions, respectively.

## IV. DESIGN AND PARAMETER IDENTIFICATION OF THE DDPI MODEL

### A. DDPI model design

PEA is widely used in micro/nanopositioning systems due to many advantages. However, its inherent hysteresis seriously affects the positioning accuracy of the manipulator. To show this issue, sinusoidal voltage signals with frequencies of 1 Hz, 10 Hz, and 20 Hz are chosen to drive the PEA under open-loop control, and the measured results are shown in Fig. 4. It can be found that when an input voltage is given, there are two corresponding displacements in the extension and retraction processes of PEA, which indicates severe hysteresis existing. In addition, the hysteresis of PEA is rate-dependent. The discrepancies of the hysteresis loop increase with the increasing operating frequencies, and it indicates that the hysteresis becomes more serious.

The traditional P-I hysteresis model consisting of parallel-connected backlash operators has been proposed and expressed as follows:

$$H_r[u](t) = \begin{cases} \max\{u(t) - r, \min\{u(t) + r, H_r[u](t - T)\}\}, & t > 0, \\ \max\{u(0) - r, \min\{u(0) + r, 0\}\}, & t = 0, \end{cases} \quad (2)$$

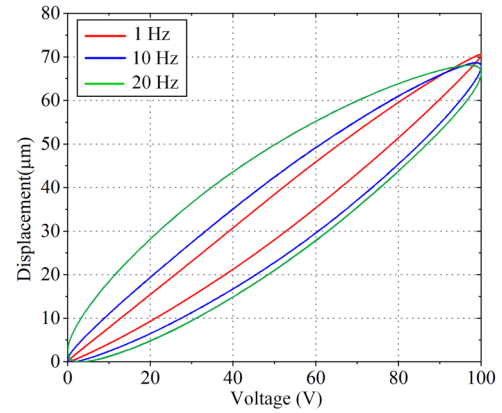


FIG. 4. Hysteresis loop of the manipulator at different frequencies.

where  $u(t)$  is the input function,  $H_r[u](t)$  and  $r$  are the output and threshold of the backlash operator, respectively, and  $T$  is the sampling period.

The shape of the hysteresis operator is centrosymmetric, but the actual PEA hysteresis loop is noncentrosymmetric. In order to obtain the asymmetric hysteresis model, dead-zone operators are introduced, which can be expressed as

$$S_d[u](t) = \begin{cases} \max\{u(t) - d, 0\} & d > 0, \\ u(t) & d = 0, \end{cases} \quad (3)$$

where  $S_d[u](t)$  and  $d$  are the output and threshold of the dead-zone operator, respectively.

Thus, the classic P-I hysteresis model can be given as

$$x(t) = \mathbf{w}_s^T S_d[\mathbf{w}_h^T \cdot \mathbf{H}_r[u](t)], \quad (4)$$

where  $x$  is the output displacement,  $u$  is the input voltage,  $\mathbf{w}_h^T = [w_{h1}, w_{h2}, \dots, w_{hm}]^T$  and  $\mathbf{w}_s = [w_{s1}, w_{s2}, \dots, w_{sn}]^T$  are the weight vectors,  $\mathbf{H}_r[u](t) = [H_{r1}[u](t), H_{r2}[u](t), \dots, H_{rm}[u](t)]^T$  and  $\mathbf{S}_d[u](t) = [S_{d1}[u](t), S_{d2}[u](t), \dots, S_{dn}[u](t)]^T$  represent backlash and dead-zone operator vectors, respectively.

The classic P-I model is rate-independent, and thus, several researchers proposed the RDPI model,<sup>28</sup> where the weight of the backlash operators changes linearly with the input rate. The linear relationship between the weight and the input rate can be given as

$$\mathbf{w}_h = \mathbf{k}\dot{u}(t) + \mathbf{b}, \quad (5)$$

where  $\mathbf{k} = [k_1, k_2, \dots, k_m]^T$  and  $\mathbf{b} = [b_1, b_2, \dots, b_m]^T$  are the slope and intercept vectors, respectively.

The hysteresis is also affected by the dynamic performance of the system. To overcome this issue, a novel DDPI model is proposed. The dynamic equations of the system have been obtained by the system identification and can be expressed as

$$G(s) = \frac{X(s)}{U(s)} = \frac{b_0}{s^2 + a_1s + a_2}. \quad (6)$$

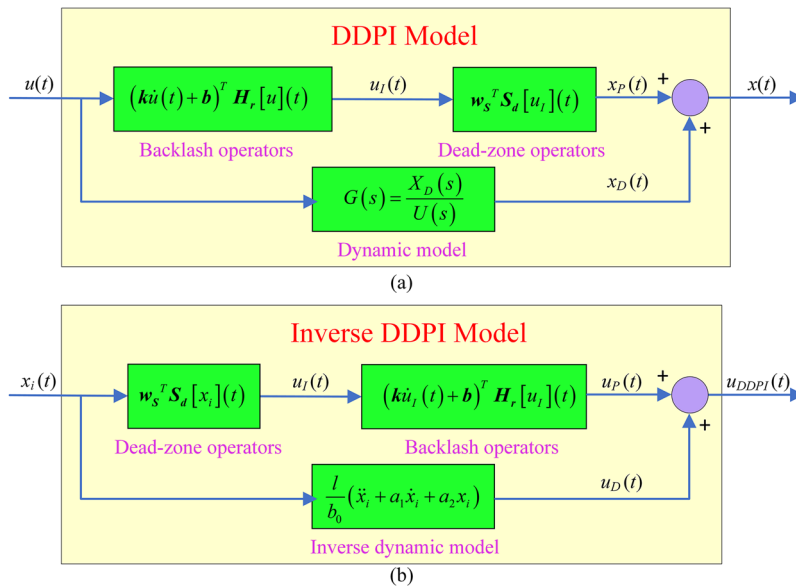


**FIG. 5.** Modified hysteresis model configuration: (a) DDPI model and (b) inverse DDPI model.

Transforming the dynamic equations of the system into differential representation,

$$\ddot{x}(t) + a_1 \dot{x}(t) + a_2 x(t) = b_0 u(t). \quad (7)$$

Thus, the impact of the dynamic performance of the system on the input can be expressed as

$$u_D(t) = \frac{l}{b_0} (\ddot{x}_i(t) + a_1 \dot{x}_i(t) + a_2 x_i(t)), \quad (8)$$

where  $x_i$  is the ideal displacement trajectory and  $l$  is the fit coefficient.

In order to reduce the hysteresis caused by the dynamic performance of the system, the dynamic equations of the system are connected in parallel to the hysteresis model. Then, the DDPI hysteresis model and the inverse model configuration can be obtained and shown in Fig. 5. Therefore, the governing equation of the DDPI

inverse hysteresis model can be given as follows:

$$u_{DDPI}(t) = \Gamma^{-1}(x_i, \dot{x}_i, \ddot{x}_i) = (k_i \dot{u}_I(t) + b)^T H_r[w_s^T \cdot S_d[x_i(t)]] + \frac{l}{b_0} (\ddot{x}_i(t) + a_1 \dot{x}_i(t) + a_2 x_i(t)). \quad (9)$$

## B. Parameter identification of DDPI model

In practical applications, it is necessary to identify the parameters of the inverse hysteresis model. The inverse operation is generally required in the traditional process of parameter identification of the hysteresis inverse model. In order to avoid the complicated inverse operation, the direct parameter identification method<sup>16</sup> is utilized to obtain the parameters of the hysteresis inverse model.

The number of operators is proportional to the model accuracy and inversely proportional to the computational speed. According

**TABLE I.** Identified parameters of the DDPI hysteresis model in the  $x$ ,  $y$ , and  $z$  directions.

$i$	$x$			$y$			$z$		
	$k_i (10^{-2})$	$b_i$	$w_{si}$	$k_i (10^{-2})$	$b_i$	$w_{si}$	$k_i (10^{-2})$	$b_i$	$w_{si}$
1	0.914	4.563	0.379	1.030	5.674	0.323	7.501	47.57	0.313
2	-1.326	-3.292	-0.028	-1.497	-4.093	-0.019	-12.10	-25.63	-0.058
3	0.356	0.462	-0.146	0.385	0.584	-0.112	3.944	1.417	-0.045
4	0.082	-0.748	0.025	0.118	-0.864	0.019	0.940	-7.892	0.011
5	0.142	-1.138	0.029	0.160	-1.324	0.008	0.009	-6.002	-0.016
6	-0.414	2.216	-0.031	-0.438	2.445	-0.026	1.259	-6.745	-4.041
7	0.172	-2.003	...	0.141	-2.138	...	-4.574	24.93	...
8	1.668	-2.931	...	1.800	-3.099	...	4.585	-35.79	...
9	-1.907	3.953	...	-1.983	4.006	...	4.641	10.02	...
10	0.370	-1.157	...	0.341	-1.174	...	-5.910	4.360	...

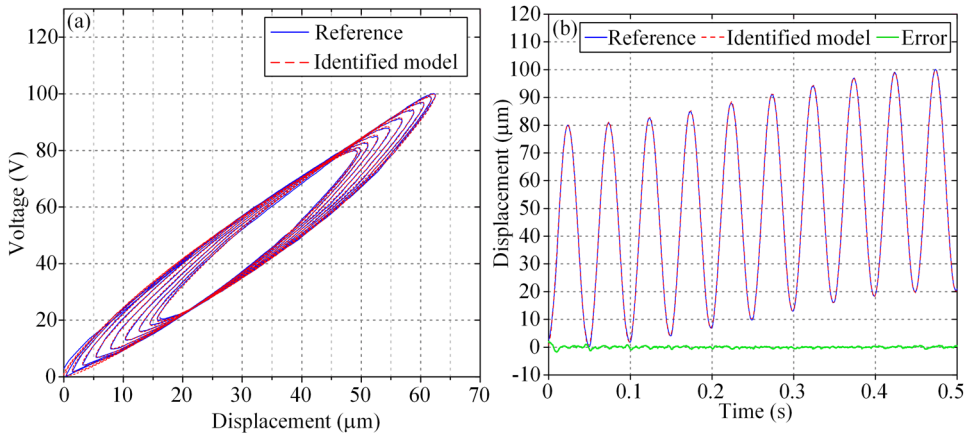


**FIG. 6.** Identification result of the DDPI model in the  $x$  direction: (a) inverse hysteresis loop; (b) time plot.

to the trial and error processes, the model accuracy and operation speed are trade-off. It is found that the 10th order backlash operators and the 6th order dead-zone operators can achieve enough model accuracy. The thresholds of the dead-zone and backlash operators are, respectively, set as

$$\begin{aligned} d &= [0, 1, 2, 3, 4, 5]^T x_{i \max} / 5, \\ r &= [0, 0.2, 0.5, 1, 3, 5, 7, 9, 9.5, 10]^T u_{I \max} / 20, \end{aligned} \quad (10)$$

where  $x_{i \max}$  is the maximum ideal displacement and  $u_{I \max}$  is the maximum intermediate voltage.

The input signal with low frequency and high frequency superposition is selected for the parameter identification so that the established hysteresis model is suitable for a high bandwidth.<sup>29</sup> The superposition signal is composed of three sinusoidal signals with the frequencies of 1 Hz, 10 Hz, and 20 Hz and can be expressed as

$$u(t) = 50 + 10 \sin\left(2\pi t - \frac{\pi}{2}\right) + \sin\left(20\pi t - \frac{\pi}{2}\right) + 40 \sin\left(40\pi t - \frac{\pi}{2}\right). \quad (11)$$

According to the least squares fit method, the objective function is set as

$$F = \|u_{DDPI} - u\|_2^2. \quad (12)$$

The three-axis identified parameters of the backlash and dead-zone operators are listed in Table I, and fit coefficients  $l$  are  $2.093 \times 10^{-2}$ ,  $3.144 \times 10^{-2}$ , and  $6.939 \times 10^{-4}$ , and fitting errors are 0.253, 0.272, and 0.217, respectively. The  $x$  direction identification result is shown in Fig. 6, indicating that the proposed DDPI hysteresis model can well match the experimental results.

## V. SMCUDE CONTROLLER DEVELOPMENT

The DDPI hysteresis model can compensate the hysteresis of the PEA, but other errors including creep and external disturbances cannot be effectively compensated. This will seriously deteriorate the performance of the micromanipulator. For the sake of high positioning accuracy of the manipulator, the hybrid feedforward/feedback

controller is developed. The SMC method is chosen as the feedback controller due to its fast response capability, which is suitable for high-frequency trajectory tracking. However, the chattering phenomenon may exist in a traditional SMC system. Recently, many research results indicate that the UDE technique has significant potential to weaken the influences of chattering and uncertain perturbation.<sup>30</sup> The key idea in the UDE-based control is to utilize the system information in the recent past to obtain an estimate of the uncertainty. Inspired by this idea, a novel SMCUDE controller is designed. According to the DDPI hysteresis model, the ideal trajectory signal is converted into a voltage signal to drive the manipulator by PEAs. Then, the output displacement is detected by a capacitive sensor in real time. In addition, the proposed SMCUDE controller is applied to adjust the voltage signal so that the actual trajectory is close to the ideal trajectory.

Considering disturbances of the system, the differential equation of the system is

$$\dot{x}(t) = Ax(t) + Bu(t) + p(u, x, t). \quad (13)$$

Then, the disturbance error can be expressed as

$$p(u, x, t) = \dot{x}(t) - Ax(t) - Bu(t). \quad (14)$$

Based on the UDE technique,<sup>31</sup> the disturbance error  $p(u, x, t)$  can be estimated by passing it through a filter. Thus, the estimated value of the disturbance error can be obtained,

$$p^*(u, x, t) = p(u, x, t) * g_f(t) = (\dot{x}(t) - Ax(t) - Bu(t)) * g_f(t), \quad (15)$$

where  $g_f(t)$  is the impulse response of a strictly proper stable filter  $G_f(s)$  with the unity gain and zero phase shift over the spectrum of  $p^*(u, x, t)$  and zero gain elsewhere. The form of the filter can be set as

$$G_f(s) = \frac{1}{1 + \tau s}, \quad (16)$$

where  $\tau$  is a time constant.

The displacement model of the system can be expressed as

$$\ddot{x} + a_1 \dot{x} + a_2 x = b_0 u + p^*(u, x, t). \quad (17)$$



The control objective is to make the actual trajectory  $x(t)$  close to the ideal trajectory  $x_i(t)$ , and the tracking error of the system can be defined as

$$e(t) = x_i(t) - x(t). \quad (18)$$

The PID-type sliding mode control surface can be represented as

$$s(t) = c_1 e(t) + c_2 \int_0^t e(\tau) d\tau + \dot{e}(t), \quad (19)$$

where  $c_i$  is positive parameter and should be chosen to satisfy the Hurwitz condition.

Design the sliding control law as

$$u_{SMCDE} = \frac{1}{b_0} [(a_1 - c_1)\dot{x} + (a_2 - c_2)x + \ddot{x}_i + c_1\dot{x}_i + c_2x_i + \lambda_1 \operatorname{sgn}(s) + \lambda_2 s - p^*], \quad (20)$$

where  $\lambda_1$  and  $\lambda_2$  are positive control gains, and  $\operatorname{sgn}(s)$  is a sign function.

To demonstrate the stability of the controller, a Lyapunov function is defined as

$$V = \frac{1}{2} s^2. \quad (21)$$

Differentiating Eq. (21) with respect to time yields

$$\begin{aligned} \dot{V} &= s\dot{s} \\ &= s(c_1\dot{e} + c_2\dot{e} + \ddot{e}) \\ &= s[c_1(\dot{x}_i - \dot{x}) + c_2(x_i - x) + \ddot{x}_i - \ddot{x}] \\ &= s[c_1(\dot{x}_i - \dot{x}) + c_2(x_i - x) + \ddot{x}_i + a_1\dot{x} + a_2x - b_0u - p^*]. \end{aligned} \quad (22)$$

Substituting Eq. (20) into Eq. (22), the following equation can be obtained:

$$\begin{aligned} \dot{V} &= s(-\lambda_1 \operatorname{sgn} s - \lambda_2 s) \\ &= -\lambda_1 |s| - \lambda_2 s^2 < 0. \end{aligned} \quad (23)$$

It can be seen that for  $|s| \neq 0$ , the derivative of the defined Lyapunov function  $\dot{V} < 0$ . When  $t \rightarrow \infty$ , the sliding mode variable  $s \rightarrow 0$ . According to Eq. (19), we can obtain  $\lim_{t \rightarrow \infty} e(t) = 0$  and  $\lim_{t \rightarrow \infty} \dot{e}(t) = 0$ . Then,  $x \rightarrow x_i$  and  $\dot{x} \rightarrow \dot{x}_i$ . Therefore, the SMCUDE controller satisfies the reachable condition and the trajectory can reach the sliding surface in a limited time, which proves the stability of the proposed controller.

Due to the change of the  $\operatorname{sgn}(s)$ , when  $s$  approaches 0, undesirable chattering may appear. In order to avoid this problem, a continuous function  $\theta(s)$  is utilized instead of  $\operatorname{sgn}(s)$ ,

$$\theta(s) = \frac{s}{|s| + \delta}, \quad (24)$$

where  $\delta$  is a very small positive constant.

Then, the sliding control law can be expressed as

$$u_{SMCDE} = \frac{1}{b_0} [(a_1 - c_1)\dot{x} + (a_2 - c_2)x + \ddot{x}_i + c_1\dot{x}_i + c_2x_i + \lambda_1 \frac{s}{|s| + \delta} + \lambda_2 s - p^*]. \quad (25)$$

Finally, the hybrid feedforward/feedback controller is established, and the schematic diagram is shown in Fig. 7. The proposed

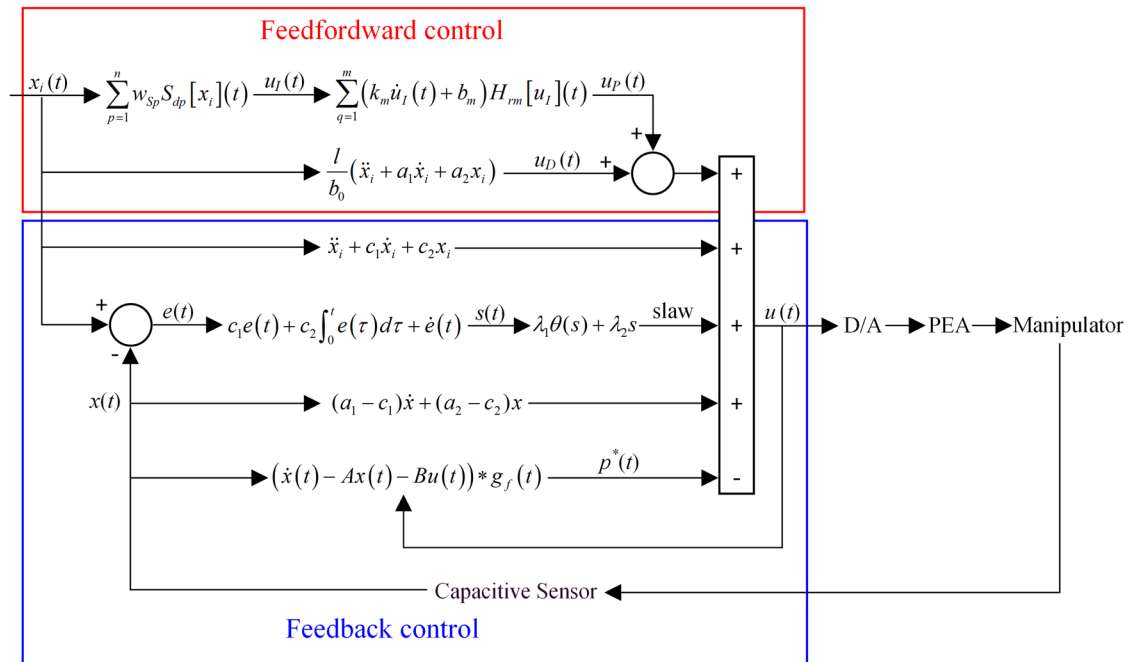


FIG. 7. Hybrid feedforward/feedback control diagram.

novel controller can reduce the effects of hysteresis, creep, and external disturbances. In addition, compared with the traditional sliding mode controller, the most remarkable feature of the controller is the ability to reduce chattering. Below, the specific application how to use the hybrid feedforward/feedback controller in the experimental measurements is introduced. In the parameter adjustment process, the number of operators in the hysteresis model should be determined first. The number of operators of the model should increase as the output displacement of the system increases. Increasing the number of operators can effectively improve the accuracy of the model, but it will reduce the calculation speed. The number of operators is constantly increased until the desired model accuracy is achieved. The coefficients of the dynamic equation have been obtained by the system parameter identification. For the feedback controller, it is necessary to adjust the proposed sliding surface parameters  $c_i$  and the approach law parameters  $\lambda_i$ . In the process of the sliding surface adjustment, the proportionality coefficient  $c_1$  is increased to improve the response feed, but a larger value will cause oscillation of the system. The integral coefficient  $c_2$  is increased to reduce the oscillation, but it will reduce the response speed. In the process of the approach law adjustment, the velocity term coefficient  $\lambda_1$  is continuously decreased and the exponential term coefficient  $\lambda_2$  is constantly increased, constantly increasing the approach speed and reducing the chattering. Based on the trial-and-error approach, controller parameters are properly turned to generate a tracking error as small as possible.

## VI. EXPERIMENT

The feedforward control experiments are first carried out to evaluate the proposed DDPI hysteresis model. Because the P-I model, RDPI model, and DDPI model have the similar structure, comparisons among them are conducted. In the comparison study, all of the models are built using the same experimental data and

**TABLE II.** Sinusoidal motion tracking errors of the three hysteresis models.

Frequency	Error ( $\mu\text{m}$ )	P-I	RDPI	DDPI
5 Hz	Maximum	2.59	1.54	1.02
	rms	0.72	0.40	0.36
20 Hz	Maximum	5.19	4.56	2.52
	rms	1.64	1.38	0.81

identification method under the same number of backlash and dead-zone operators, and the working frequencies are set as 5 Hz and 20 Hz, respectively.

The tracking results and the position errors of the three hysteresis models at different frequencies are shown in Fig. 8. For a clear presentation, the maximum and root-mean-square (rms) tracking errors of the three hysteresis models are tabulated in Table II. It can be seen that the accuracy of the DDPI model is slightly better than the RDPI model for the frequency of 5 Hz, and the accuracies of both models are much higher than the traditional P-I model. The tracking errors of the DDPI model are 50.8% and 12.1% times less than those of the P-I model and the RDPI model, respectively. However, the accuracy of the three models will drop at a high frequency of 20 Hz. Among these models, the accuracies of the P-I model and the RDPI model drop sharply. The tracking errors of the DDPI model are 50.7% and 41.6% times less than those of the P-I model and RDPI model, respectively. Thus, it can be concluded that the RDPI model and the DDPI model can greatly improve the accuracy of the traditional P-I model at low operating frequencies. However, in the case of high operating frequencies, the performance of the RDPI model is extremely degraded and only the DDPI model can still maintain high precision, which verifies the effectiveness and accuracy of the DDPI model.

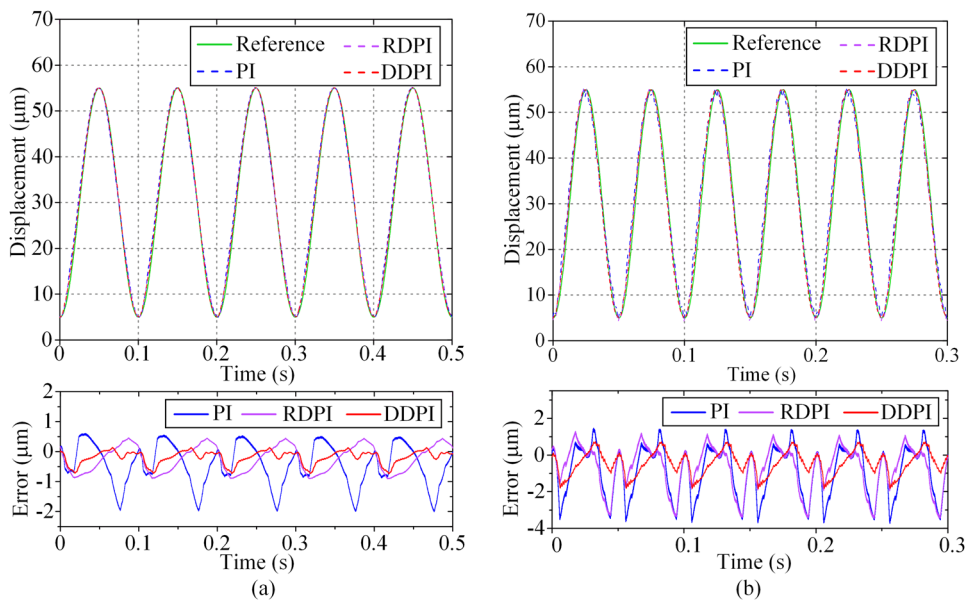


**FIG. 8.** Comparison among the P-I model, RDPI model, and DDPI model at (a) 5 Hz and (b) 20 Hz.

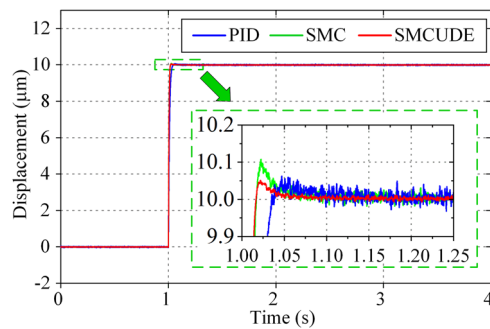


FIG. 9. Step response results of PID, SMC, and SMCUDE.

Through hysteresis model experimental tests, it can be observed that the DDPI model can reduce the hysteresis characteristic to some extent, but the trajectory tracking accuracy is still not ideal at high operating frequencies. In order to further improve control accuracy and reduce the effects of the external disturbances, the hybrid feedforward/feedback control is adopted. To verify the validity of the proposed SMCUDE controller, the PID, traditional SMC, and SMCUDE controllers are combined with the DDPI hysteresis model to form three feedforward/feedback controllers for comparison studies.

Step response was investigated and the desired displacement trajectory was defined as a step signal with a final value as  $10\text{ }\mu\text{m}$ . All controllers are tuned to obtain transient response as quick as possible and overshoot as small as possible. The step response results are shown in Fig. 9, and the corresponding performance parameters are tabulated in Table III. It can be found that the SMC controller can improve the response speed by 37% in comparison with the PID controller; however, the overshoot will also increase. The proposed SMCUDE controller has a close settling time to the SMC controller, but the corresponding overshoot is only 0.51%, which indicates that the SMCUDE controller can improve the response speed without loss of stability. In addition, the SMCUDE controller enhances the rms steady-state error by 45% and 33% in comparison with the PID and SMC controller, respectively.

The motion tracking of a 20 Hz sinusoidal trajectory has been examined for three controllers, and the results are shown in Fig. 10. Due to the low response speed, the measured trajectory of the PID controller obviously lags behind the ideal trajectory and thus leads to large trajectory tracking error, which can be well reduced by the SMC controller. However, the traditional SMC controller produces a strong chattering phenomenon due to the discontinuous switching control action, as shown in Fig. 10(b), which will deteriorate

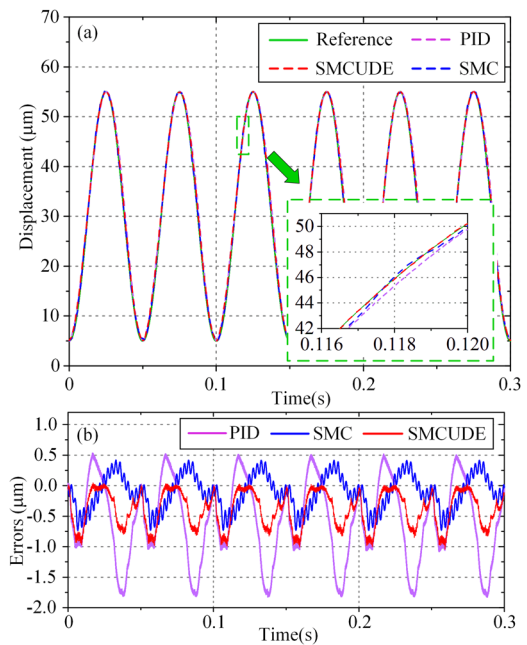


FIG. 10. Sinusoidal motion tracking results. (a) Position tracking results. (b) Position tracking error.

the positioning accuracy of the positioner. The proposed SMCUDE controller can effectively avoid chattering and reduce external disturbance. Quantitatively, the PID, SMC, and SMCUDE controller create the rms errors of 0.77, 0.49, and  $0.31\text{ }\mu\text{m}$ , respectively. The accuracy of SMCUDE has improved by 60% and 37% in comparison with PID and SMC controllers, respectively. The motion tracking of the 20 Hz sinusoidal trajectory demonstrates that the proposed feedforward/feedback hybrid controller can achieve well fast precision positioning.

## VII. CONCLUSION

This paper developed the methodologies for the modeling and control of a piezoactuated XYZ micromanipulator toward fast precision positioning. Based on the frequency response approach, the system dynamic model was obtained. A DDPI hysteresis model including backlash operators, dead-zone operators, and the system dynamic model has been established to achieve hysteresis compensation. The direct parameter identification method is utilized to avoid the complicated inverse operation and obtain the hysteresis inverse model. Compared with the P-I model, RDPI model through trajectory tracking tests, the proposed DDPI model shows higher positioning accuracy at high operating frequencies, which can be attributed to the consideration of manipulator dynamic performance. The effectiveness of the developed DDPI can be confirmed.

In order to avoid creep and external disturbances, a novel SMCUDE controller based on the sliding mode control as well as the uncertainty and disturbance estimation technique is added to form a hybrid feedforward/feedback controller. The developed controller has fast response capability and strong robustness to further

TABLE III. Step response performance parameters of the three controllers.

Parameters	PID	SMC	SMCUDE
Settling time (ms)	121	72	68
Maximum overshoot (%)	0.63	1.08	0.51
Steady-state error (RMS) ( $\mu\text{m}$ )	0.011	0.009	0.006

improve fast precision positioning performance. The step response shows that the settling time is 68 ms, the overshoot is 0.51%, and the steady-state error is  $0.006\text{ }\mu\text{m}$  under the proposed control strategy. Compared with the traditional SMC, the SMCUDE controller can improve the response speed without loss of stability. Finally, the sinusoidal trajectory track was carried out to demonstrate that fast precision positioning can be achieved with an RMS error of  $0.31\text{ }\mu\text{m}$  and the influences of chattering can be reduced by utilizing the SMCUDE controller.

## ACKNOWLEDGMENTS

This research was supported by the National Natural Science Foundation of China (Grant Nos. 51675371, 51675367, and 51675376), National Key R&D Program of China (Grant Nos. 2016YFE0112100, 2017YFB1104700, and 2017YFE0112100), and EU H2020 Program MNR4SCell (Grant No. 734174).

## REFERENCES

- <sup>1</sup>Y. Qin, B. Shirinzadeh, Y. Tian, D. Zhang, and U. Bhagat, "Design and computational optimization of a decoupled 2-DOF monolithic mechanism," *IEEE/ASME Trans. Mechatronics* **19**(3), 872–881 (2014).
- <sup>2</sup>F. Wang, C. Liang, Y. Tian, X. Zhao, and D. Zhang, "Design and control of a compliant microgripper with a large amplification ratio for high-speed micro manipulation," *IEEE/ASME Trans. Mechatronics* **21**(3), 1262–1271 (2016).
- <sup>3</sup>A. Colom, I. Casuso, F. Rico, and S. Scheuring, "A hybrid high-speed atomic force-optical microscope for visualizing single membrane proteins on eukaryotic cells," *Nat. Commun.* **4**, 2155 (2013).
- <sup>4</sup>B. Gozen and O. Ozdoganlar, "Design and evaluation of a mechanical nanomanufacturing system for nanomilling," *Precis. Eng.* **36**(1), 19–30 (2012).
- <sup>5</sup>K. Cai, Y. Tian, X. Liu, S. Fatikow, F. Wang, L. Cui, D. Zhang, and B. Shirinzadeh, "Modeling and controller design of a 6-DOF precision positioning system," *Mech. Syst. Signal. Process.* **104**, 536–555 (2018).
- <sup>6</sup>M. Ling, J. Cao, Z. Jiang, M. Zeng, and Q. Li, "Optimal design of a piezo-actuated 2-DOF millimeter-range monolithic flexure mechanism with a pseudo-static model," *Mech. Syst. Signal. Process.* **115**, 120–131 (2019).
- <sup>7</sup>Y. Qin, B. Shirinzadeh, Y. Tian, and D. Zhang, "Design issues in a decoupled XY stage: Static and dynamics modeling, hysteresis compensation, and tracking control," *Sens. Actuators, A* **194**, 95–105 (2013).
- <sup>8</sup>K. Cai, Y. Tian, X. Liu, D. Zhang, J. Shang, and B. Shirinzadeh, "Development and control methodologies for 2-DOF micro/nano positioning stage with high out-of-plane payload capacity," *Rob. Comput.-Integr. Manuf.* **56**, 95–105 (2019).
- <sup>9</sup>Q. Xu, "Precision motion control of piezoelectric nanopositioning stage with chattering-free adaptive sliding mode control," *IEEE Trans. Autom. Sci. Eng.* **14**, 238–248 (2017).
- <sup>10</sup>G. Gu, L. Zhu, C. Su, H. Ding, and S. Fatikow, "Modeling and control of piezo-actuated nanopositioning stages: A survey," *IEEE Trans. Autom. Sci. Eng.* **13**(1), 313–332 (2016).
- <sup>11</sup>L. Liu, K. Tan, S. Chen, C. Teo, and T. Lee, "Discrete composite control of piezoelectric actuators for high-speed and precision scanning," *IEEE Trans. Ind. Inf.* **9**(2), 859–868 (2013).
- <sup>12</sup>K. Cai, Y. Tian, F. Wang, D. Zhang, X. Liu, and B. Shirinzadeh, "Design and control of a 6-degree-of-freedom precision positioning system," *Rob. Comput.-Integr. Manuf.* **44**, 77–96 (2017).
- <sup>13</sup>M. A. Janaideh, S. Rakheja, and C. Su, "An analytical generalized Prandtl-Ishlinskii model inversion for hysteresis compensation in micropositioning control," *IEEE/ASME Trans. Mechatron.* **16**(4), 734–744 (2011).
- <sup>14</sup>Z. Guo, Y. Tian, X. Liu, B. Shirinzadeh, F. Wang, and D. Zhang, "An inverse Prandtl-Ishlinskii model based decoupling control methodology for a 3-DOF flexure-based mechanism," *Sens. Actuators, A* **230**, 52–62 (2015).
- <sup>15</sup>W. Ang, P. Khosla, and C. Riviere, "Feedforward controller with inverse rate-dependent model for piezoelectric actuators in trajectory-tracking applications," *IEEE/ASME Trans. Mechatronics* **12**(2), 134–142 (2007).
- <sup>16</sup>Y. Qin, Y. Tian, D. Zhang, B. Shirinzadeh, and S. Fatikow, "A novel direct inverse modeling approach for hysteresis compensation of piezoelectric actuator in feedforward applications," *IEEE/ASME Trans. Mechatronics* **18**(3), 981–989 (2013).
- <sup>17</sup>L. Tian, Z. Xiong, J. Wu, and H. Ding, "A new rate-dependent model for high-frequency tracking performance enhancement of piezoactuator system," *Smart Mater. Struct.* **26**(5), 055008 (2017).
- <sup>18</sup>W. Zhu, Z. Zhu, P. Guo, and B. Ju, "A novel hybrid actuation mechanism based XY nanopositioning stage with totally decoupled kinematics," *Mech. Syst. Signal. Process.* **99**, 747–759 (2018).
- <sup>19</sup>Q. Xu and M. Jia, "Model reference adaptive control with perturbation estimation for a micropositioning system," *IEEE Trans. Control Syst. Technol.* **22**(1), 352–359 (2014).
- <sup>20</sup>Y. Li and Q. Xu, "Design and robust repetitive control of a new parallel-kinematic XY piezostage for micro/nanomanipulation," *IEEE/ASME Trans. Mechatronics* **17**(6), 1120–1132 (2012).
- <sup>21</sup>T. Dinh and K. Ahn, "Radial basis function neural network based adaptive fast nonsingular terminal sliding mode controller for piezo positioning stage," *Int. J. Control, Autom. Syst.* **15**(6), 2892–2905 (2017).
- <sup>22</sup>C. Liang, F. Wang, B. Shi, Z. Huo, K. Zhou, Y. Tian, and D. Zhang, "Design and control of a novel asymmetrical piezoelectric actuated microgripper for micromanipulation," *Sens. Actuators, A* **269**, 227–237 (2018).
- <sup>23</sup>Y. Zhang and Q. Xu, "Adaptive sliding mode control with parameter estimation and kalman filter for precision motion control of a piezo-driven microgripper," *IEEE Trans. Control Syst. Technol.* **25**(2), 728–735 (2017).
- <sup>24</sup>J. Mishra, Q. Xu, X. Yu, and M. Jalili, "Precision position tracking for piezoelectric-driven motion system using continuous third-order sliding mode control," *IEEE/ASME Trans. Mechatronics* **23**(4), 1521–1531 (2018).
- <sup>25</sup>S. Li, H. Du, and X. Yu, "Discrete-time terminal sliding mode control systems based on Euler's discretization," *IEEE Trans. Autom. Control* **59**(2), 546–552 (2014).
- <sup>26</sup>C. Liang, F. Wang, Y. Tian, X. Zhao, and D. Zhang, "Development of a high speed and precision wire clamp with both position and force regulations," *Rob. Comput.-Integr. Manuf.* **44**, 208–217 (2017).
- <sup>27</sup>Q. Zhong and D. Rees, "Control of uncertain LTI systems based on an uncertainty and disturbance estimator," *J. Dyn. Syst., Meas., Control* **126**(4), 905–910 (2004).
- <sup>28</sup>M. A. Janaideh, C. Su, and S. Rakheja, "Development of the rate-dependent Prandtl-Ishlinskii model for smart actuators," *Smart Mater. Struct.* **17**(3), 035026 (2008).
- <sup>29</sup>C. Liang, F. Wang, Y. Tian, X. Zhao, and D. Zhang, "Grasping force hysteresis compensation of a piezoelectric-actuated wire clamp with a modified inverse Prandtl-Ishlinskii model," *Rev. Sci. Instrum.* **88**(11), 115101 (2017).
- <sup>30</sup>B. Kurkcu, C. Kasnakoglu, and M. Efe, "Disturbance/uncertainty estimator based integral sliding-mode control," *IEEE Trans. Autom. Control* **63**(11), 3940–3947 (2018).
- <sup>31</sup>B. Ren, Q. Zhong, and J. Chen, "Robust control for a class of non-affine nonlinear systems based on the uncertainty and disturbance estimator," *IEEE Trans. Ind. Electron.* **62**(9), 5881–5888 (2015).